Pergamon

Int. J. Heat Mass Transfer. Vol. 37, No. 17, pp. 2635–2646, 1994

0017–9310/94 $7.00+0.00

0017–9310(94)E0106–5

Radiative enhancement of tube-side heat transfer

K. H. IM and R. K. AHLUWALIA†

Argonne National Laboratory, 9700 South Cass Avenue, Argonne, IL 60439-4841, U.S.A.

(*Received* 10 *November* 1993 *and in final form* 18 *March* 1994)

Abstract—The potential of augmenting film coefficient by uniformly dispersing thin metallic/ceramic filaments oriented longitudinally along a tube is investigated. The purpose of the rigidly held filaments is to create a participating medium from a gas otherwise transparent to thermal radiation. The filaments absorb the thermal radiation emitted by the tube and transfer the heat convectively to the flowing gas. Wave theory shows that optical thickness >10 can be achieved with 50 μm SiC filaments at 300 cm^{-2} number density in a 2.54 cm diameter tube. Solution of the radiation transport equation indicates that the radiative film coefficients are a function of filament material, diameter and number density, and gas and surface temperatures.

1. INTRODUCTION

IN MANY industrial applications involving heat transfer from hot flue gases to a clean gas/air flowing inside the tubes, it is desirable to improve the tube-side (film) heat transfer coefficient (h_i). Improvement in the film coefficient not only leads to reduction in heat transfer area, but also lowers the tube temperature. Sometimes the metallurgical advantages associated with operating at lower tube temperatures can far outweigh the economy of heat transfer area.

In designing combustion equipment, it is generally good practice to maintain, when possible, a film coefficient much greater than the outside heat transfer coefficient (h_o). With $h_i > h_o$, the tube-wall temperature is closer to the temperature of colder clean gas flowing inside the tube than to the temperature of the flue gas on the outside walls. If the flue gas contains aggressive contaminants, the attendant problems of corrosion and fouling are more manageable at lower tube temperatures. In any case, the outside heat transfer coefficient is often limited by pressure drop considerations as in heat recuperators for glass melting and steel making processes or by erosion considerations as in a coal combustion environment. Thus, in order to improve the overall heat transfer coefficient (U) the only available option is to raise h_i as high as possible within the constraints applicable to the tube-side flow.

In fluidized bed combustors, the outside heat transfer coefficient is very high such that U becomes limited by h_i. Thus, there is an inherent incentive to seek means of enhancing the film coefficient for tubes embedded in the fluidized beds.

Ceramic heat exchangers are being developed to indirectly heat compressed air to turbine inlet temperatures (1523 K and higher) in a coal-fueled furnace. At these temperatures, the heat exchanger can be made more compact if it is configured to utilize radiation rather than convection as the principal mode of heat transfer. Depending on combustion gas and surface temperatures, the heat transfer coefficients for radiation in coal furnaces can be 600–1200 W m^{-2} K^{-1} compared to 50–100 W m^{-2} K^{-1} obtainable with convective cross-flow heat exchangers (5.08 cm diameter, 1.25–1.5 staggered tube spacing to diameter ratio, 10 m s^{-1} face velocity). On the other hand, the convective tube-side heat transfer coefficient for air in smooth tubes at 500 K may not exceed 55–325 W m^{-2} K^{-1} in the 10^4–10^5 Reynolds number range. Thus, there is a critical need to enhance h_i if the concept of radiative heat exchanger is to be viable.

There exists an extensive literature on techniques of augmenting tube-side heat transfer coefficients [1]. For gases, the popular techniques include use of rough surfaces, extended surfaces and tube inserts. These are capable of achieving 10–70% augmentation in film coefficients. The conventional techniques principally rely on convective augmentation and incur an offsetting penalty of increased pressure drop or material cost. Generally, the fractional increase in pressure drop is greater than the fractional increase in film coefficient. We propose an alternative technique of augmenting the film coefficient using radiative means. Normally, radiation is not an effective mode of tube-side heat transfer because the mean beam length is small (2.54–7.62 cm) and because the gas may be transparent to thermal radiation. To create a participating medium, we disperse thin filaments uniformly and longitudinally inside the tubes. The filaments are held rigidly and may be woven into a mesh using few transverse filaments. The filaments are

†Author to whom correspondence should be addressed.

NOMENCLATURE

A	face area
d	filament diameter
D	tube diameter
h	heat transfer coefficient
H	Hankel function
I	radiation intensity
J	Bessel function
k	absorption index
n	refractive index
N	filament number density
Q	heat flux
Q_a, Q_e, Q_s	efficiency factors for absorption, emission and scattering
r	radial coordinate
T	temperature
V	nodal volume
w	weight factor
x	size parameter.

Greek symbols

β	extinction coefficient
ε_w	wall emissivity
λ	wavelength
μ, η	directional cosines
ν	frequency
τ	optical thickness
ϕ	phase function
ω	scattering albedo
Ω	solid angle.

Subscripts

b	black body
c	convection
g	gas
r	radiation
w	wall.

heated radiatively by the tube surface and, thereafter, transfer heat convectively to the flowing gas inside the tubes. The filaments are nearly isothermal with the gas by virtue of a high coefficient of heat transfer between the filaments and gas and the extended surface area obtained with the use of thin filaments.

This paper discusses aspects related to radiative heat transfer from tube surface to gas inside the tube containing stationary rigid filaments, dispersed uniformly and oriented principally in the longitudinal direction. Section 2 deals with the optical properties of the filament materials and radiation cross sections for extinction and scattering. Section 3 applies the discrete ordinate method to solving the radiation transport equation in a cylindrical participating medium. Section 4 develops the heat balance equations for extracting film coefficients from the solution of radiation transport equation. Finally, Section 5 attempts to quantify the augmentation in film coefficient obtainable with the use of thin filaments.

2. RADIATION CROSS SECTIONS

Cross sections for absorption and scattering by long thin filaments may be determined by examining the solution of the scalar wave equation applied to normally-illuminated infinitely long cylinders [2]. Two sets of solutions (I and II) are available depending on the polarization plane of the incident electric field. If the incident light is unpolarized, the efficiencies for scattering and extinction must be averaged.

$$Q_s = \tfrac{1}{2}(Q_{s,I} + Q_{s,II}) \tag{1}$$

$$Q_e = \tfrac{1}{2}(Q_{e,I} + Q_{e,II}). \tag{2}$$

The efficiency factors are available in the form of infinite series functionally dependent on the size parameter (x) and the complex refractive index of the cylinder material relative to the medium refractive index (m).

$$Q_{s,I} = \frac{2}{x}\left(|b_0|^2 + 2\sum_{l=1}^{\infty}|b_l|^2\right) \tag{3}$$

$$Q_{e,I} = \frac{2}{x}\mathrm{Re}\left(b_0 + 2\sum_{l=1}^{\infty} b_l\right) \tag{4}$$

$$Q_{s,II} = \frac{2}{x}\left(|a_0|^2 + 2\sum_{l=1}^{\infty}|a_l|^2\right) \tag{5}$$

$$Q_{e,II} = \frac{2}{x}\mathrm{Re}\left(a_0 + 2\sum_{l=1}^{\infty} a_l\right) \tag{6}$$

where

$$a_l = \frac{[D_l(mx)/m + l/x]\,J_l(x) - J_{l-1}(x)}{[D_l(mx)/m + l/x]\,H_l^{(1)}(x) - H_{l-1}^{(1)}(x)} \tag{7}$$

$$b_l = \frac{[mD_l(mx) + l/x]\,J_l(x) - J_{l-1}(x)}{[mD_l(mx) + l/x]\,H_l^{(1)}(x) - H_{l-1}^{(1)}(x)} \tag{8}$$

$$D_l(\rho) = \frac{J_l'(\rho)}{J_l(\rho)}. \tag{9}$$

The filaments may be made from metals, alloys or ceramics. A comprehensive compilation of complex refractive indices of these materials is available in the form of a handbook [3, 4]. Figure 1 contains a graphical presentation of the data extracted from this reference for a metal (iron). In the infrared and visible, the metals typically have high values of refractive and absorption indices. Figure 1 also shows the corresponding room-temperature data for hexagonal sili-

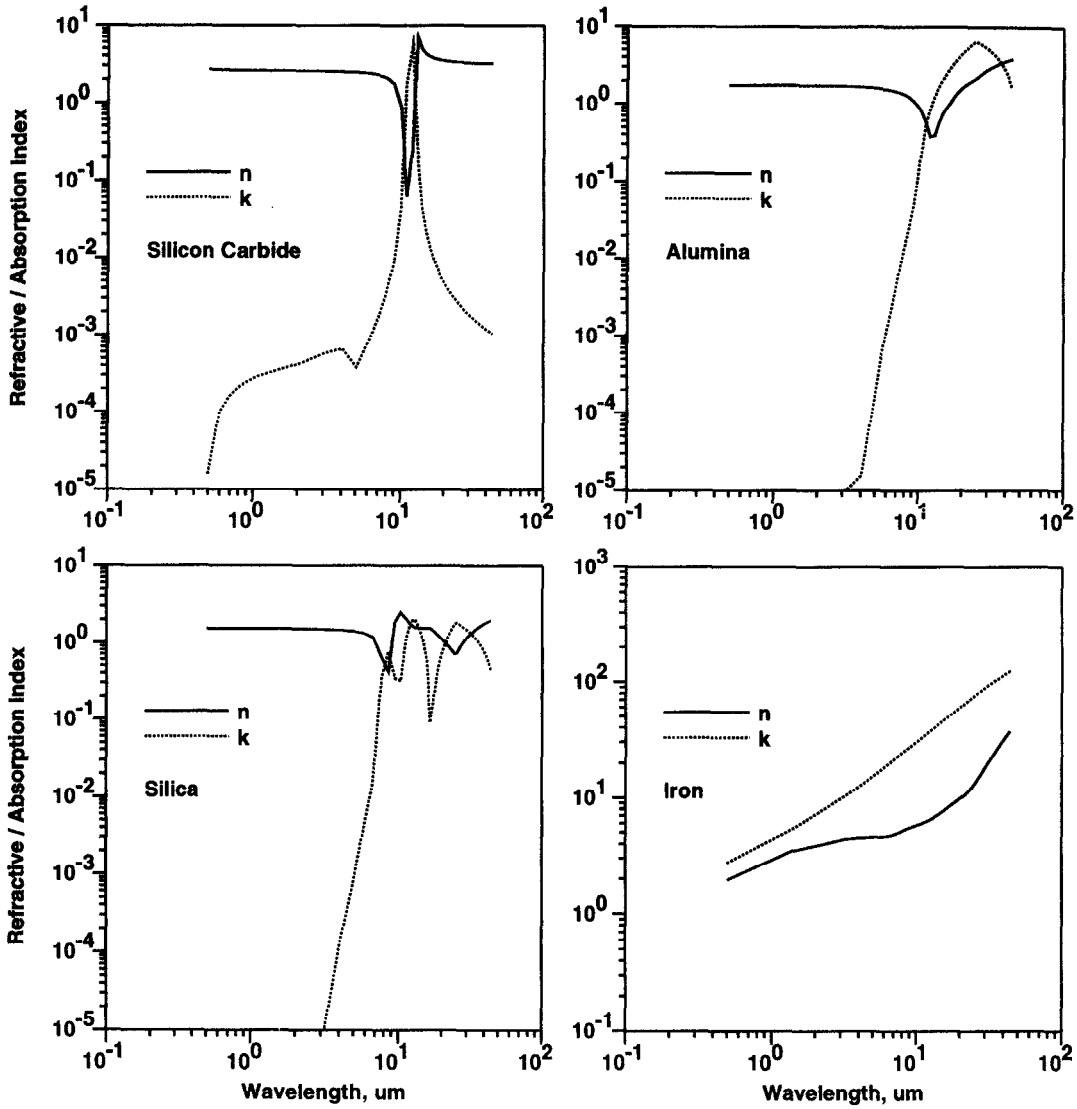

FIG. 1. Refractive indices of silicon carbide, silica, alumina and iron in the infrared.

con carbide in the infrared range. In the 2–22 μm region, the reststrahlen reflection data are well fitted with an oscillator model of the form

$$(n-ik)^2 = \varepsilon_\infty \left[1 + \frac{\omega_L^2 - \omega_T^2}{\omega_T^2 - \omega^2 + i\Gamma\nu}\right] \quad (10)$$

with $\omega_L = 969\ \text{cm}^{-1}$, $\omega_T = 793\ \text{cm}^{-1}$, $\Gamma = 4.76\ \text{cm}^{-1}$, and $\varepsilon_\infty = 6.7$.

Recently a physically-based mathematical model, OPTPROP, has been developed at the Applied Physics Laboratory to calculate the complex refractive indices of solids over large frequency and temperature ranges [5, 6]. The computer code contains models for one-phonon absorption, multi-phonon sum band absorption, Urbach tail, weel absorption tail free carrier, Sallmeier (for room temperature), and empirical scattering models for many optical materials. Results obtained from applying this code to alumina and silica at 1300 K are displayed in Fig. 1. Although not shown on the log–log plots, the broadening of absorption spectra at elevated temperatures has been observed and is of special interest since it represents the possibility of increased attenuation. Note that alumina and silica have absorption indices $< 10^{-5}$ for wavelengths < 3 μm. Thus a significant part of wall-emitted radiation will not be usefully absorbed by filaments made from these materials.

Figure 2 displays the efficiency factors for absorption and scattering as calculated from the wave theory and the refractive indices data of Fig. 1. Of the four materials considered, the efficiency factors for SiC are most sensitive to filament diameter and least sensitive for iron. Within the range of 50–1000 μm filament diameters, the efficiency factor for absorption by SiC filaments increases with d whereas that for scattering decreases with d at all wavelengths. Thus, the larger

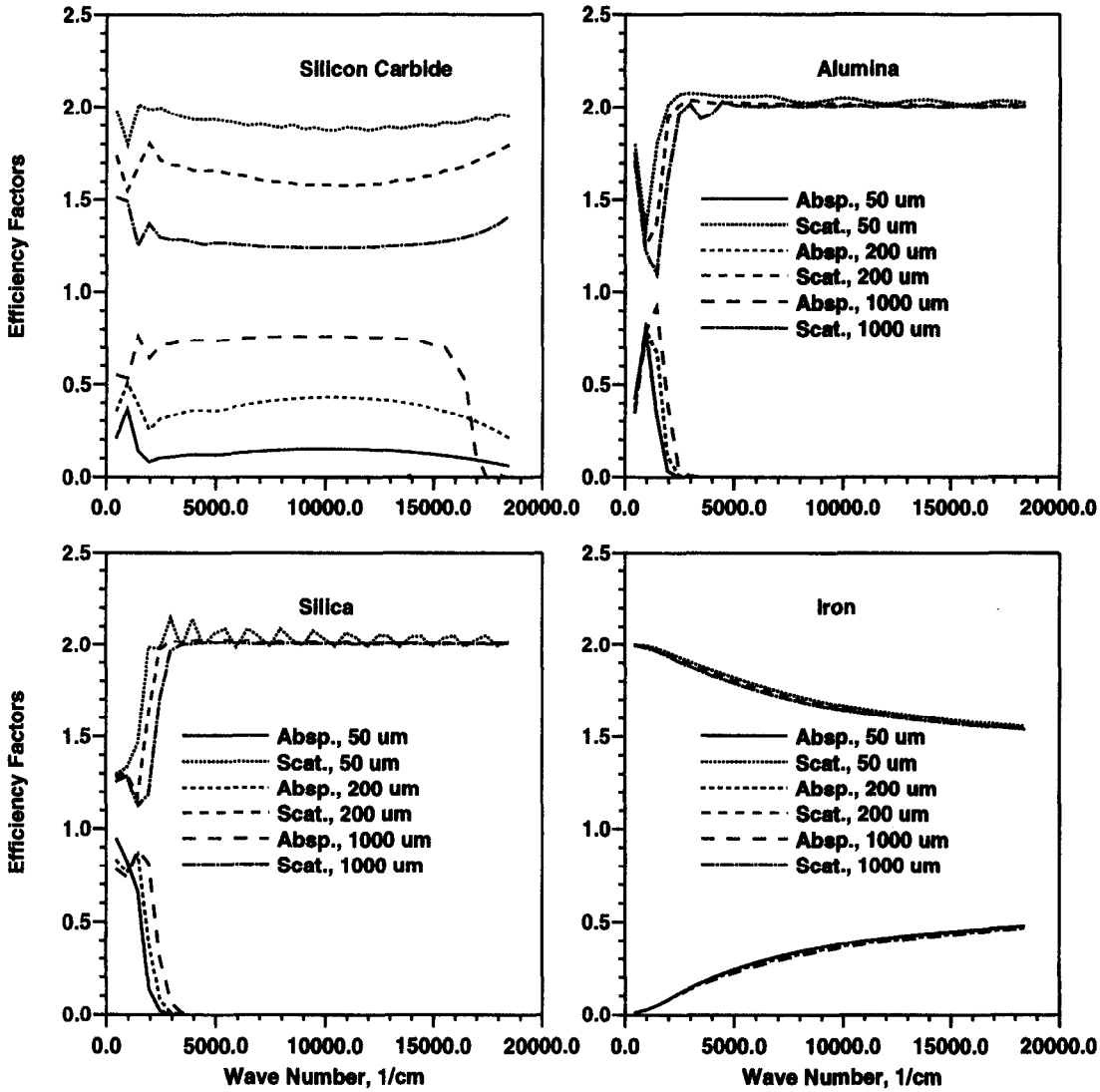

FIG. 2. Efficiency factors for absorption and scattering by silicon carbide, silica, alumina and iron filaments of different diameters.

the diameter of SiC filaments, the smaller the scattering albedo. Over the IR range, the frequency-averaged scattering albedo decreases from ~ 0.95 at $d = 50$ μm to 0.65 at $d = 1000$ μm. Alumina and silica filaments display similar trends in that Q_a increases and Q_s decreases with diameter, although the extent of variation is much smaller. Consistent with the absorption spectra, Q_a for silica and alumina filaments is vanishingly small for wavelengths < 3 μm and Q_s oscillates about the asymptotic limit of 2.

Given Q_a and Q_s, the extinction coefficient and scattering albedo for unimodal size distribution of filaments can be calculated as

$$\beta_v = (Q_a + Q_s)\pi dN \tag{11}$$

$$\omega_v = Q_a/(Q_a + Q_s). \tag{12}$$

The filament diameters of interest are sufficiently large such that the size parameter x ($= \pi d/\lambda$) $\gg 1$ and the extinction efficiency factor $(Q_a + Q_s)$ approaches the asymptotic limit of 2. Equation (11) then indicates that one can obtain an extinction coefficient of 9.4 cm^{-1} by using 50 μm filaments at a number density of 300 cm^{-2} or 1000 μm filaments at 15 cm^{-2}. If these filaments are dispersed in a 2.54 cm diameter tube, the optically thick limit ($\beta_v D = 23.9$) is reached with a porosity $(1 - \pi d^2 N/4)$ of 99.4% for 50 μm filaments and 88.2% for 1000 μm filaments. If silicon carbide is used as filament material, then radiation transport will be dominated by scattering for 50 μm filaments although considerable absorption of wall-emitted radiation should occur since the optical thickness based on Q_a is also greater than 1. For 200 μm SiC filaments, absorption and scattering will contribute equally to attenuation.

3. RADIATION TRANSPORT

Consider radiation transport in an absorbing, emitting, anisotropically scattering, cylindrical pipe medium bounded by diffusely emitting-reflecting walls. Approximating the medium as long and narrow ($\partial I_v/\partial z = 0$), the radiation transport equation (RTE) simplifies to

$$\frac{\mu}{r}\frac{\partial(rI_v)}{\partial r}+\frac{1}{r}\frac{\partial(\eta I_v)}{\partial \phi}+\beta_v I_v=(1-\omega_v)\beta_v I_{bv}+\frac{\omega_v\beta_v}{4\pi}\int_{4\pi}\Phi(\Omega,\Omega')\,I_v(r,\Omega')\,d\Omega' \quad (13)$$

subject to the wall boundary condition

$$I_v(\boldsymbol{r},\boldsymbol{\Omega})=\varepsilon_w I_{bv}+\frac{(1-\varepsilon_w)}{\pi}\int_{\mathbf{n}\cdot\boldsymbol{\Omega}'<0}|\boldsymbol{n}\cdot\boldsymbol{\Omega}'|\,I(\mathbf{r},\boldsymbol{\Omega}')\,d\Omega' \qquad \mathbf{n}\cdot\boldsymbol{\Omega}>0 \quad r=R. \quad (14)$$

Following Carlson and Lathrop [7], we use the S_4 discrete ordinate method for solving the RTE. We employ a finite-difference grid in which point p denotes the center and i and $i+1$ the faces of the node i. We multiply equation (13) by $2\pi r\,dr\,dz$, integrate over the volume element and drop the subscript v for convenience in presentation. For direction l with $\mu_l > 0$, one obtains

$$\mu_l(A_{i+1}I^l_{i+1}-A_iI^l_i)-(A_{i+1}-A_i)\times(\alpha_{l+1/2}I_p^{l+1/2}-\alpha_{l-1/2}I_p^{l-1/2})/w_l=-\beta_iV_pI^l_p+(1-\omega_i)\beta_iV_pI_{bp}+\omega_i\beta_iV_pI_s \quad (15)$$

where

$$I_s=\frac{1}{4\pi}\sum_{l'}\phi_{ll'}I^{l'}_pw_{l'} \quad (16)$$

$$\alpha_{l+1/2}=\alpha_{l-1/2}+w_l\mu_l. \quad (17)$$

The intensities $I^l_i, I^l_{i+1}, I_p^{l+1/2}$ and $I_p^{l-1/2}$ can be expressed in terms of the intensity at the node center by using an interpolation factor δ.

$$I^l_p=\delta I^l_{i+1}+(1-\delta)I^l_i=\delta I_p^{l+1/2}+(1-\delta)I_p^{l-1/2}. \quad (18)$$

Substituting equation (18) into (13) and gathering terms

$$I^l_p=\frac{\mu_lAI^l_i-\alpha/w_l(A_{i+1}-A_i)I_p^{l-1/2}+\delta\beta_iV_p[(1-\omega_i)I_{bp}+\omega_iI_s]}{\mu_lA-\alpha/w_l(A_{i+1}-A_i)+\delta\beta_iV_p} \quad (19)$$

where

$$\alpha=(1-\delta)\alpha_{l+1/2}+\delta\alpha_{l-1/2} \quad (20)$$

$$A=(1-\delta)A_{i+1}+\delta A_i. \quad (21)$$

A similar equation can be derived for directions with $\mu_l < 0$. Equation (19) is solved for intensity at the node center by traversing the grid in the beam direction.

Table 1. Quadrature coefficients

l	Direction cosine μ_l	Direction weight w_l
1	−1.0	0
2	−0.908248	2.0943951
3	−0.295876	4.1887902
4	0.295876	2.0943951
5	0.908248	4.1887902

For positive directional cosines (see Table 1), the traverse is started using the center boundary condition:

$$I^l_p=I^{l'}_p \quad \mu_l=-\mu_{l'} \quad r=0. \quad (22)$$

For beams with negative directional cosines, the traverse is started at the wall using the diffuse reflection boundary condition:

$$I^l_p=\varepsilon_wI_b+\frac{(1-\varepsilon_w)}{\pi}\sum_{\mu_{l'}>0}\phi_{ll'}I^{l'}_pw_{l'} \quad \mu_l<0 \quad r=R. \quad (23)$$

The beam $\mu_l = -1$ is a special direction with zero weight and zero α. It is convenient to initiate the solutions for different beam directions starting from $\mu_l = -1$ and in the order listed in Table 1. Knowing I^l_p, equation (18) provides a method for obtaining intensity at the downstream face through extrapolation. Thus, a recursive loop can be set up in which the intensities are updated by marching along the beam directions. The process is continued until the change in calculated intensities over successive iterations becomes smaller than the prescribed tolerance.

4. RADIATION HEAT TRANSFER

Given radiation intensity, the spectral radiative heat flux at the tube wall can be calculated from

$$Q_{wv}=\sum_l\mu_lw_lI^l_p(R,\mu_l). \quad (24)$$

Knowing Q_{wv}, the radiative heat transfer coefficient h_r can be defined by performing spectral integration

$$h_r=\frac{1}{(T_g-T_w)}\int_0^\infty Q_{wv}\,dv. \quad (25)$$

The spectral integration is carried out by dividing the infrared spectrum into 37 bands. Each band is subdivided into 20 frequencies. Equations (1) and (2) are used to calculated the extinction and scattering efficiency factors for each frequency and summed to obtain band-averaged values of the extinction coefficient and scattering albedo. Knowing β_v and ω_v, RTE is solved for each band to obtain Q_{wv}.

For specified gas and tube temperatures, the filament temperature distribution can be determined from the following heat balance.

$$\int_0^\infty \nabla \cdot Q_\nu \, d\nu = \pi d N h_f (T_f - T_g) \tag{26}$$

where

$$\nabla \cdot Q_\nu = (1-\omega_\nu)\beta_\nu (4\pi I_{b\nu} - \sum w_l I_p^l). \tag{27}$$

An iterative procedure is required to solve equation (26) since $I_{b\nu}$ should be evaluated at the local filament temperature rather than the known gas temperature. Moreover, since I_p is also a function of $I_{b\nu}$ the iteration process has to extend over the radiation transport equation as well. For sufficiently large number density, the difference between filament and gas temperatures $(T_f - T_g)$ becomes negligibly small, and the iteration procedure becomes unnecessary.

An analogy with longitudinal flow between cylinders/tubes arranged in a regular array is invoked to estimate the convective heat transfer coefficient (h_f) between the filaments and gas. The Nusselt number $(Nu_d = h_f d/k)$ for fully-developed laminar flow is a function only of pitch-to-diameter ratio (P/d). Following Sparrow *et al.* [8], Nu_d for a triangular arrangement of cylinders is calculated as 9.7, 4.5, 2.7, 2.0, 1.5, 1.3, 1.1 and 0.84 at P/d equal to 1.4, 2, 3, 4, 6.5, 8, 11 and 20, respectively. For fully-developed turbulent flow, the concept of hydraulic diameter of an infinite array is used to define d_e as

$$\frac{d_e}{d} = a\left(\frac{P}{d}\right)^2 - 1 \tag{28}$$

where $a = 2\sqrt{3}/\pi$ for a triangular arrangement and $4/\pi$ for a square arrangement of tubes. The Nusselt number, Nu_{d_e}, may then be estimated from standard correlations for pipe flow as a function of Prandtl number and Reynolds number based on d_e.

5. RESULTS AND DISCUSSION

A number of calculations have been performed to investigate the extent of enhancement in radiative heat transfer obtainable with thin filaments. For convenience of comparison with the convective counterpart, results are presented in the form of radiative heat transfer coefficient h_r defined in equation (25). Particular attention is paid to the dependence of h_r on filament diameter, filament number density, filament material, wall temperature and the difference between wall and gas temperatures. Although results are presented for one tube diameter (2.54 cm), $\varepsilon_w = 0.9$ and one flow rate corresponding to a Reynolds number of 2×10^4 at $T_w = 600$ K, h_r for other tube diameters can be inferred by recognizing the functional dependence of h_r on the optical thickness and the scattering albedo. Thus, for the same filament diameter and material and gas and wall temperatures, h_r is merely a function of the product Nd.

Plotted in Fig. 3 are the radiative heat transfer coefficients with silicon carbide filaments for a range of filament diameters (50–1000 μm), filament number densities (5–600 cm^{-2}), wall temperatures (600–1600 K), and the difference in wall and gas temperatures (50–300 K). As is characteristic of radiation transport, h_r increases monotonically with wall temperature and inversely with $T_w - T_g$. It is also a strong function of filament diameter and number density. The dependence of h_r on N and d can best be understood through the effects of these parameters on absorption coefficient and h_f. As indicated in Fig. 2 and equation (11), at constant Nd, the absorption coefficient increases and the scattering albedo decreases with filament diameter. In general, the higher the absorption coefficient and the lower the scattering albedo, the higher the h_r. At constant Nd, the pitch-to-diameter ratio P/d varies inversely as the square root of filament diameter. In laminar flow, it can be readily shown that Nu_d bears an inverse relationship with P/d such that, at constant Nd, h_f is only weakly dependent on the filament diameter. In turbulent flow the relationship is a bit more complex. In the limit of $P/d \gg 1$, it can be shown that the hydraulic diameter d_e, and hence Re_{d_e}, is only a function of Nd. Thus, at constant Nd and $P/d \gg 1$, turbulent h_f is independent of the filament diameter. The combined effect of absorption coefficient increasing with d, and h_f being nearly independent of d is that at constant Nd, h_r is higher with thicker filaments.

Within the selected range of parameters, Fig. 3 shows h_r to vary between 7.5–30 W m^{-2} K^{-1} at $T_w = 600$ K and 86–554 W m^{-2} K^{-1} at $T_w = 1600$ K. Under the same conditions, the flow Reynolds number varies from 1.1×10^4 at $T_w = 1600$ K to 3.8×10^4 at $T_w = 600$ K to give a convective heat transfer coefficient for air lying between 77–145 W m^{-2} K^{-1}. Thus, under most favorable conditions ($d = 1000$ μm, $N = 30$ cm^{-2}) the filaments serve to enhance the total heat transfer coefficient by 40% at $T_w = 600$ K and 382% at $T_w = 1600$ K.

The temperature differential between the filaments and gas can be estimated from the h_r data presented in Fig. 2.

$$T_f - T_g = \left(\frac{h_r}{\pi d N h_f}\right)(T_w - T_g). \tag{29}$$

The temperature differential $(T_f - T_g)$ can be regarded as a measure of convective resistance to the overall radiative heat transfer. Need for increasing the filament number density may be indicated if $(T_f - T_g)$ is a substantial fraction of $(T_w - T_g)$. As an example, $(T_f - T_g)$ is 77 K for $d = 1000$ μm, $T_w = 1600$ K, $T_w - T_g = 100$ K and $N = 5$ cm^{-2}. The temperature drop reduces to 55 K on increasing N to 10 cm^{-2}, 28 K at $N = 20$ cm^{-2} and 15 K at $N = 30$ cm^{-2}. The heat transfer coefficient (h_r) correspondingly improves from 142 W m^{-2} K^{-1} at $N = 5$ cm^{-2} to 284 at $N = 10$ cm^{-2}, 463 at $N = 20$ cm^{-2} and 554 at 30 cm^{-2}.

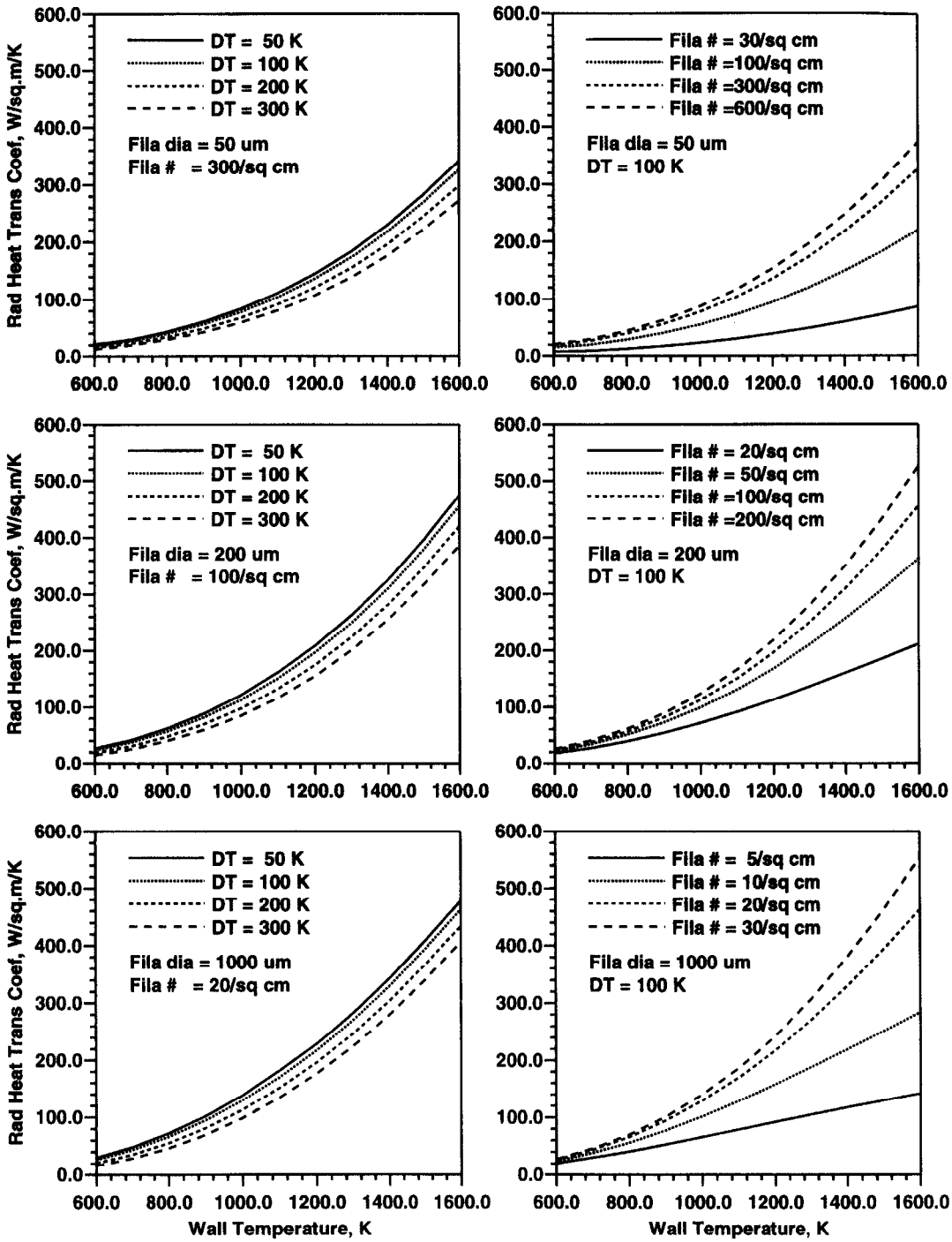

FIG. 3. Radiative heat transfer coefficients with SiC filaments dispersed in a 2.54 cm diameter pipe. The mass flow rate of air is held constant so that the Reynolds number, reference value = 2.1×10^4 at 550 K, varies with temperature. $\varepsilon_w = 0.9$.

Figures 4 and 5 present the calculated radiative heat transfer coefficients for silica and alumina filaments. Much higher h_r values are obtained with filaments made of silica rather than alumina, although both significantly underperform silicon carbide filaments. Unlike SiC filaments, h_r with SiO_2/Al_2O_3 filaments is almost independent of $T_w - T_g$ especially at high wall temperatures. Like SiC filaments, for the same *Nd*, higher radiative heat transfer coefficients are obtained with thicker filaments.

Figure 6 provides an indication of the radiative enhancement in heat transfer coefficient achievable with filaments made from metals and metallic alloys. The optical constants of iron have been used as ref-

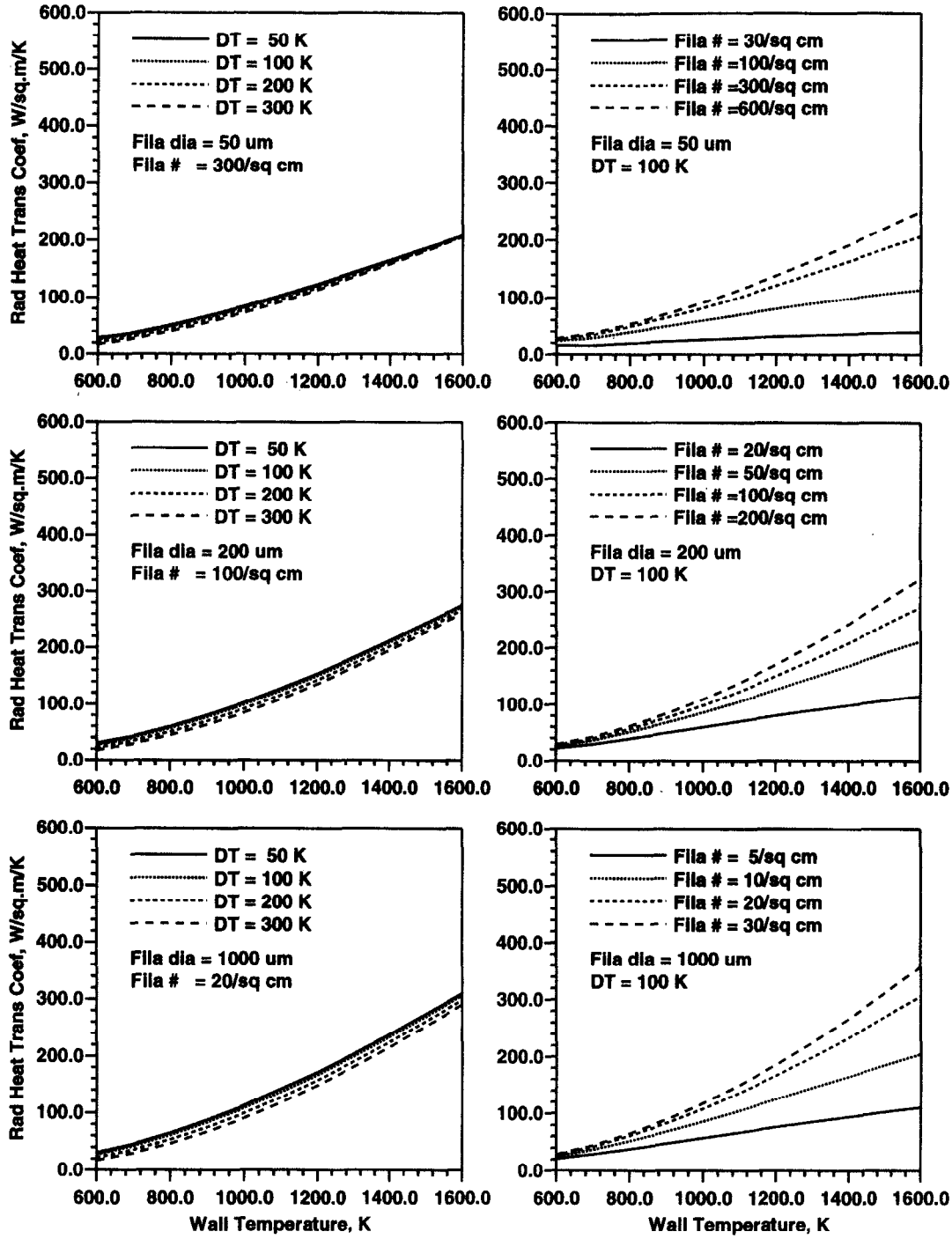

FIG. 4. Radiative heat transfer coefficients with SiO_2 filaments dispersed in a 2.54 cm diameter pipe.

erence in these calculations. For comparison with ceramic filaments, results are presented for wall temperatures beyond the suitability limits for metals and alloys. These show that metallic filaments perform almost as well as silicon carbide filaments and much better than silica or alumina filaments. A major difference in metallic and SiC filaments is in the dependence of h_r on d. Given the insensitivity of efficiency factors of metallic filaments to diameter (see Fig. 2), the absorption coefficient is only a function of Nd and scattering albedo is independent of diameter. Thus, at constant Nd, h_r is similar in magnitude with thick and thin filaments. The trends in variation of h_r with T_w and $T_w - T_g$ are identical to those with silicon carbide filaments.

It is of interest to assess the penalty in pressure drop incurred by the use of filaments. The Fanning friction factor (f_F) for laminar pressure drop due to filaments

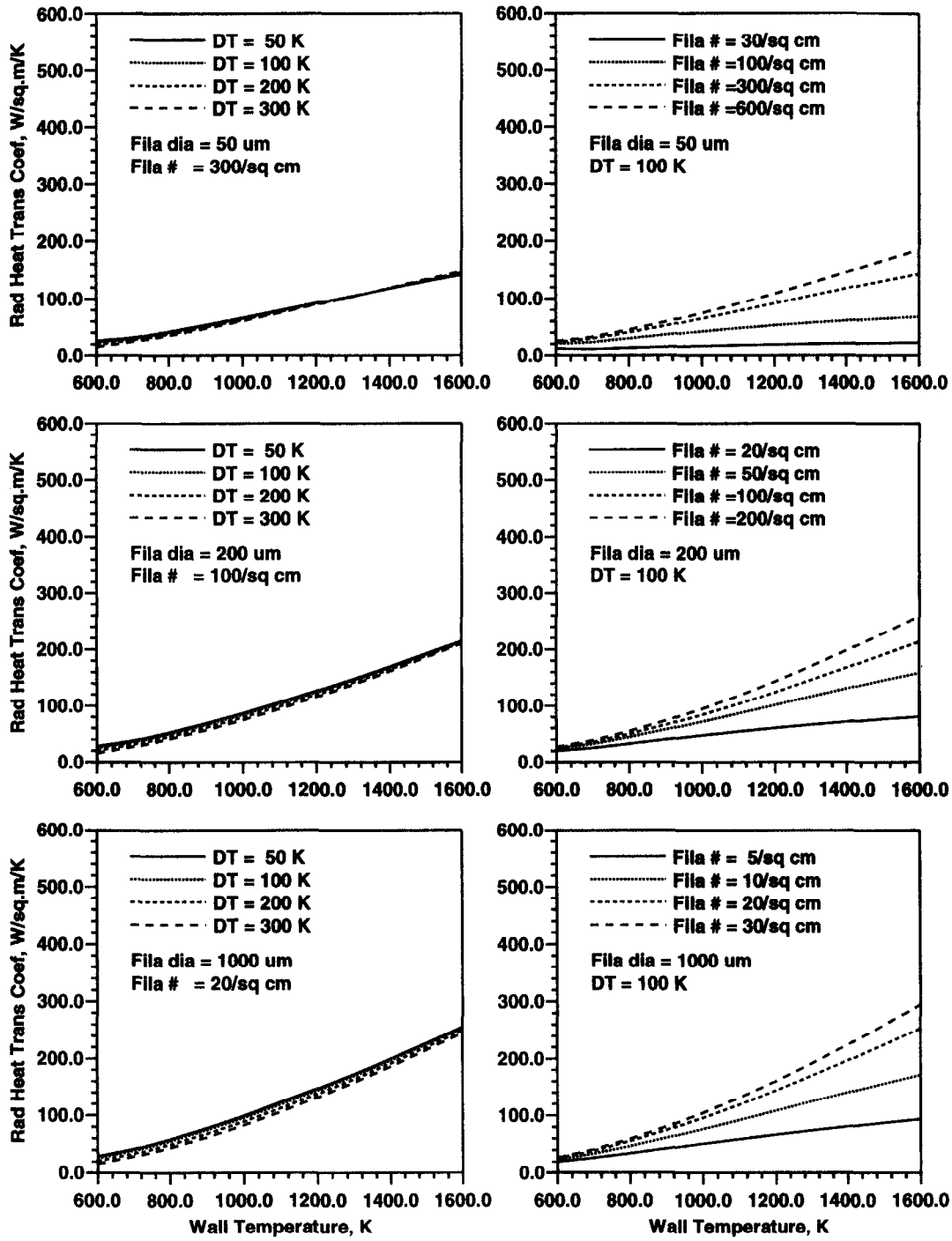

FIG. 5. Radiative heat transfer coefficients with Al_2O_3 filaments dispersed in a 2.54 cm diameter pipe.

can be estimated from the following formula derived from the work of Sparrow and Loeffler [9].

$$f_F = \left(\frac{1-\varepsilon}{\varepsilon}\right)\frac{f'(\varepsilon)}{Re_D}\frac{D^2}{d^2}. \quad (30)$$

In the above equation, ε is the porosity given as $1-\pi d^2 N/4$, and $f'(\varepsilon)$ admits values of 21, 15, 10, 7 and 5 at ε equal to 0.6, 0.7, 0.8, 0.9 and 0.95, respectively, for a triangular array. For a square array, the corresponding values of $f'(\varepsilon)$ are 17.5, 13.5, 10, 7 and 5. It can be shown that the Fanning friction factor for turbulent pressure drop due to filaments is given by the following equation.

$$f_F = \left(\frac{1-\varepsilon}{\varepsilon}\right)\frac{D}{d}f(Re_{d_e}) \quad (31)$$

where $f(Re_{d_e})$ is the friction factor for smooth pipes corresponding to Reynolds number based on d_e.

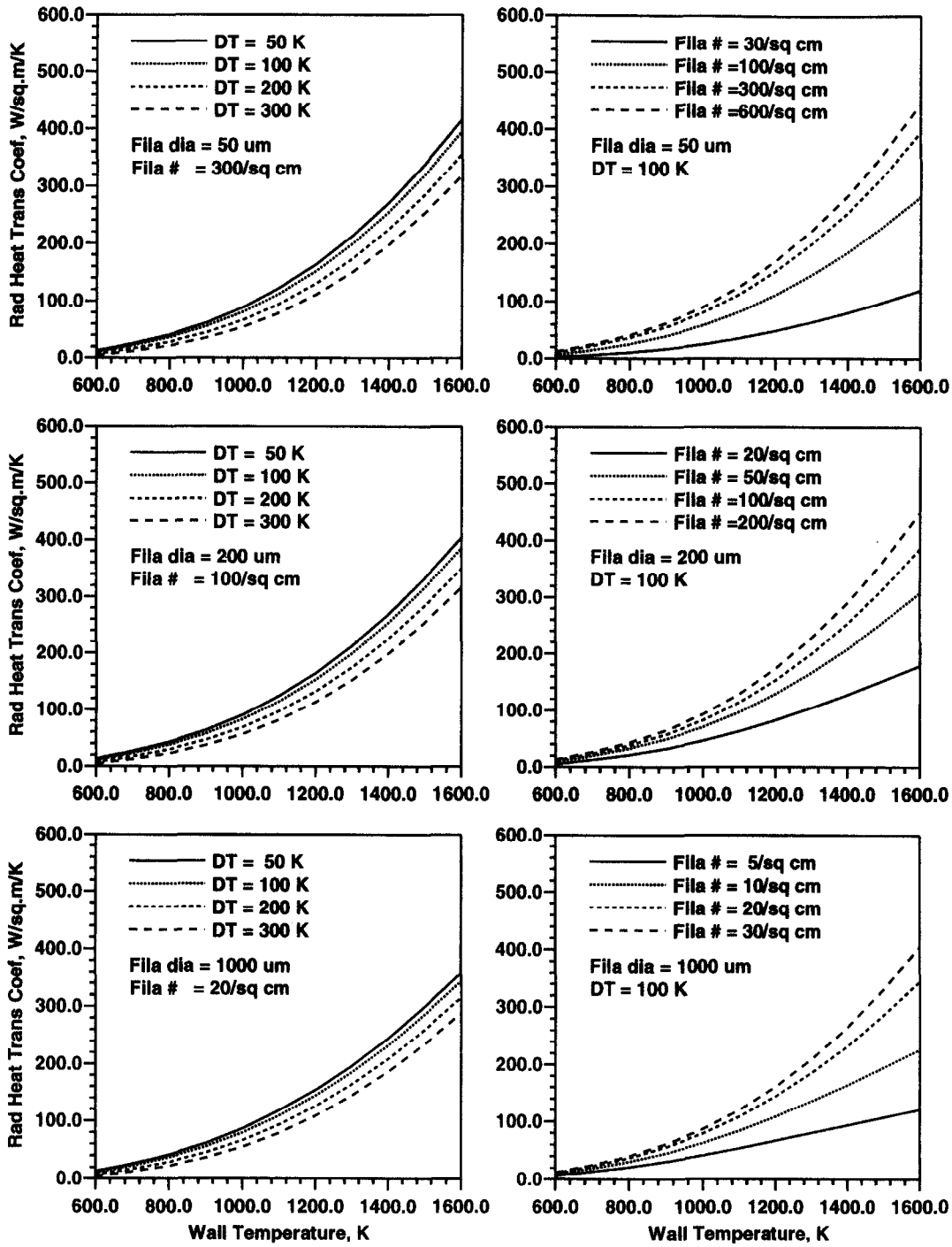

FIG. 6. Radiative heat transfer coefficients with metallic filaments dispersed in a 2.54 cm diameter pipe.

Figure 7 plots the friction factor (f_F) for pressure drop due to filaments relative to the friction factor ($f(Re_D)$) for pipe flow at the same Reynolds number based on pipe diameter D. Results are presented as a function of porosity for a 2.54 cm diameter pipe, three filament diameters (200, 500 and 1000 μm) and two flow Reynolds numbers (10^4 and 10^5). To place the results in a proper perspective, the radiative heat transfer coefficients for SiC filaments are also presented in the same figure corresponding to $T_w = 1600$ K and $T_w - T_g = 100$ K. It is seen that for a given porosity (d^2N), thinner filaments lead to higher heat transfer coefficients, but with disproportionately higher relative friction factors. Alternately, for a specified radiative heat transfer coefficient and Re_D, thicker filaments incur a smaller penalty in the relative friction factor but at a lower porosity, implying a higher d^2N.

Although the pipe flow is turbulent, i.e.

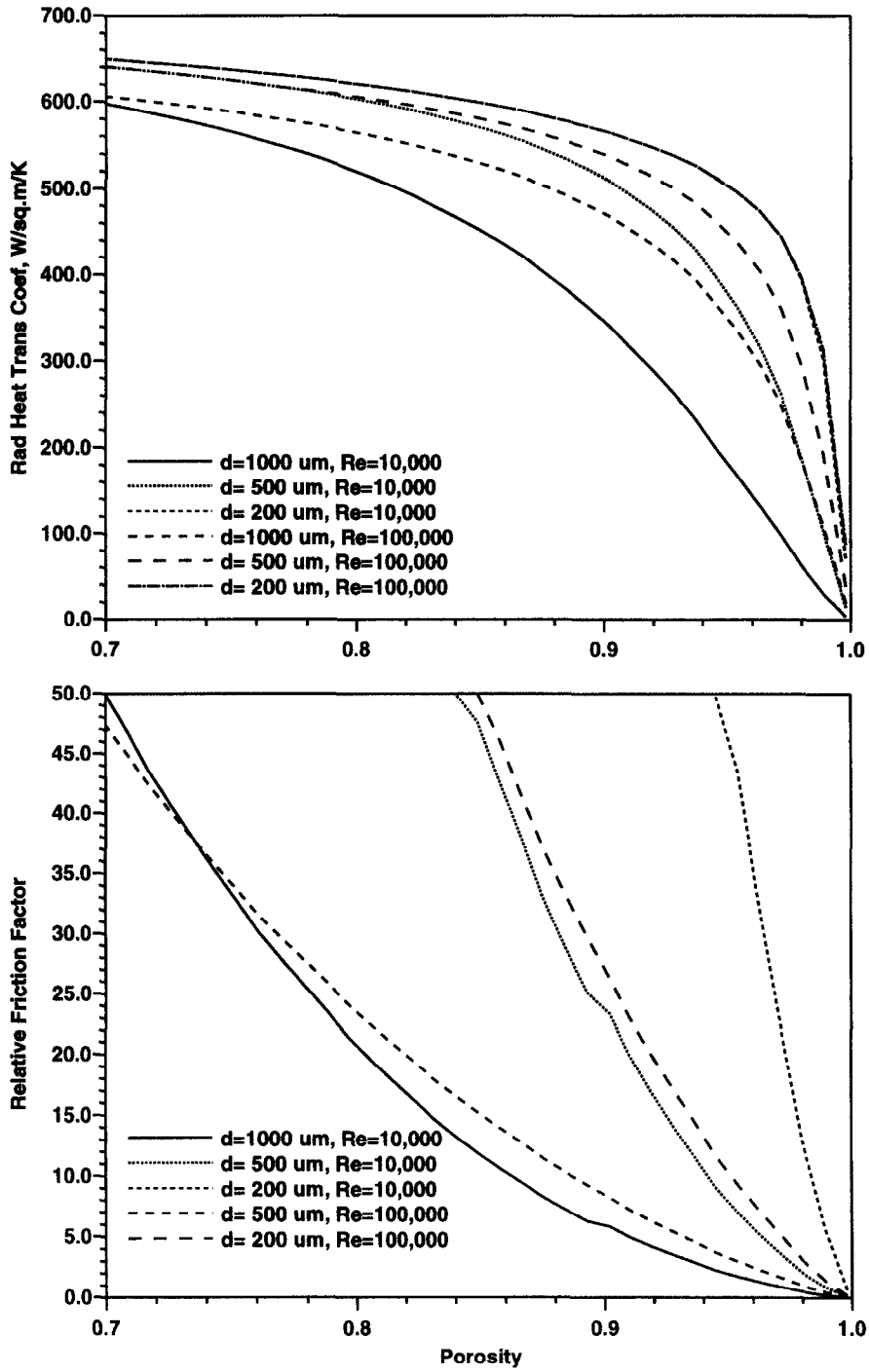

FIG. 7. Radiative heat transfer coefficients and friction factors for silicon carbide filaments dispersed in a 2.54 cm diameter pipe at $T_w = 1600$ K, $T_g = 1500$ K and $\varepsilon_w = 0.9$.

$Re_{d_c} \gg 2000$, the filament flow may be laminar as judged from Re_{d_c}. For a smooth transition from laminar to turbulent flow, the filament flow is regarded as laminar if f_F calculated from equation (30) exceeds f_F calculated from equation (31) and turbulent if vice versa. Based on this criterion, flow parallel to 200 μm filaments corresponding to $Re_D < 10^5$ and $\varepsilon > 0.7$ is considered to be laminar. Since the Nusselt number in laminar flow is independent of Reynolds number, so is the radiative heat transfer coefficient as shown in Fig. 7. However, the relative friction factor, $f_F/f(Re_D)$, for 200 μm filaments decreases sharply with Re_D since f_F is inversely proportional to Re_D whereas f varies as $1/Re_D^{0.2}$. If the filament flow is turbulent, as for 1000

μm filaments, the radiative heat transfer coefficient increases with Re_D whereas the relative friction factor decreases by a factor determined by $f(Re_{d_c})/f(Re_D)$.

6. ASSESSMENT AND CONCLUSIONS

The concept of dispersing thin filaments inside a tube to create a participating medium thereby promoting radiative heat exchange has been presented. The physical, geometrical, flow and thermal parameters that affect radiative heat transfer have been identified and their influence assessed. The important parameters are optical constants of filament materials; filament diameter, number density and arrangement; and flow Reynolds number, wall temperature and the temperature differential between the wall and gas. These parameters affect radiative heat transfer through efficiency factors for absorption and scattering, radiation transport and the coefficient for convective heat transfer between the filaments and flowing gas. Application of wave theory for normally illuminated cylinders, along with the complex refractive indices data, indicates that SiC is the most suitable filament material followed by metals and alloys, SiO_2 and Al_2O_3. For SiC materials, the thicker the filaments, the higher the radiative heat transfer coefficient. Similar dependence of h_r on filament diameter has been observed for SiO_2 and Al_2O_3 filaments. For metallic filaments, the radiative heat transfer coefficient somewhat decreases with filament diameter.

As is characteristic of radiation transport, the potential for augmentation in heat transfer is greatest at high wall temperatures. Thus, the filaments are most suitable as promoters of heat transfer in high-temperature applications such as air preheaters in MHD plants and ceramic heat exchangers for indirectly fired gas-turbine cycles. The augmentation is naturally a function of filament number density as is the incremental pressure drop due to the filaments. There exists a natural trade-off between the augmentation in heat transfer and the associated penalty in pressure drop. The trade-off can best be resolved by carrying out an analysis of the form shown in Fig. 7 for any particular application being considered.

Acknowledgement—This work was supported by the U.S. Department of Energy, Pittsburgh Energy Technology Center, under Contract W-31-109-Eng-38.

REFERENCES

1. Y. Mori, A. E. Sheindlin and N. Afgan (Editors), *High Temperature Heat Exchangers*, pp. 39–59. Hemisphere, Washington, DC (1986).
2. C. F. Bohren and D. R. Huffman, *Absorption and Scattering of Light by Small Particles*, pp. 194–205. Wiley, New York (1983).
3. E. D. Palik (Editor), *Handbook of Optical Constraints of Solids* II, pp. 385–396, Academic Press, New York (1991).
4. E. D. Palik (Editor), *Handbook of Optical Constraints of Solids*, pp. 587–595, Academic Press, New York (1985).
5. M. E. Thomas, A computer code for modeling optical properties of window materials. In *Windows and Dome Technologies and Materials, Proc. SPIE*, Vol. 1112, pp. 260–267. SPIE, Bellingham, WA (1989).
6. W. J. Tropf and M. E. Thomas, Models of optical properties of solids. In *Window and Dome Technologies and Materials, Proc. SPIE*, Vol. 1760. SPIE, Bellingham, WA (1992).
7. B. G. Carlson and K. D. Lathrop, Transport theory—the method of discrete ordinates. In *Computing Methods in Reactor Physics*. Gordon and Breach Science Publishers, New York (1968).
8. E. M. Sparrow, A. L. Loeffler, Jr and H. A. Hubbard, Heat transfer to longitudinal laminar flow between cylinders *ASME J Heat Transfer* 415–422 (1961).
9. E. M. Sparrow and A. L. Loeffler, Jr, Longitudinal laminar flow between cylinders arranged in regular array *A.I.Ch.E. Jl* **5**, 325–330 (1959).